Band bowing and the direct-to-indirect crossover in random BAlN alloys

Jimmy-Xuan Shen, Darshana Wickramaratne, and Chris G. Van de Walle

Phys. Rev. Materials **1**, 065001 — Published 13 November 2017

DOI: 10.1103/PhysRevMaterials.1.065001

Band bowing and the direct-to-indirect crossover in random BAlN alloys

Jimmy-Xuan Shen
Department of Physics, University of California, Santa Barbara, California 93106-9530, USA

Darshana Wickramaratne and Chris G. Van de Walle
Materials Department, University of California, Santa Barbara, California 93106-5050, USA

(Dated: October 19, 2017)

Boron-containing nitride alloys such as BAlN are being explored as novel members of the nitride family of materials for electronic and optoelectronic applications. Using hybrid density functional calculations we determine structural properties, band gaps and band-gap bowing of random wurtzite BAlN alloys. The fundamental band gap of BN is indirect while AlN is a direct-band-gap semiconductor. This leads to a crossover in the band gap from direct to indirect at 28% boron. We find that the direct band gap experiences extreme bowing, leading to a fundamental gap that changes very little up to 17% boron incorporation.

I. INTRODUCTION

Ternary alloys based on wurtzite AlN, GaN and InN have enabled the development of light-emitting diodes,[1] laser diodes[2] and high-power electronics.[3] Large-band-gap nitride alloys are required to push optoelectronic devices into the ultraviolet (UV) spectrum, and large polarization discontinuities at the interface of III-nitride heterostructures would enable devices that host high-density two-dimensional electron gases (2DEGs). Use of boron nitride as a member of the III-nitride family may help in achieving these goals. Wurtzite BN is predicted to have the largest spontaneous polarization[4] among the III-nitrides.[5] Alloying boron into AlN could expand the range of band gaps and polarization charges that can be accessed by alloys of the III-nitrides, making BAlN alloys a promising material for an array of technological applications.

The ground state of BN is hexagonal,[6] but the wurtzite phase [see Fig. 1(a)] is of high interest in light of experimental efforts to alloy boron at low concentrations into wurtzite AlN using metal-organic vapor phase epitaxy (MOVPE)[7] or molecular beam epitaxy (MBE).[8,9] While the large lattice mismatch between BN and AlN leads to a large miscibility gap,[10] BAlN alloys are still expected to be stable in the wurtzite phase[7] for low boron concentrations. Given the potential technological impact of BAlN alloys, it is essential to know their structural and electronic properties and how they compare to those of the parent compounds, AlN and BN.

Since BN is not stable in the wurtzite phase, no experimental information is available to enable predictions of the properties of wurtzite BAlN alloys, highlighting the importance of predictive first-principles calculations. The electronic structure of zinc-blende[11–13] and wurtzite[14] BAlN alloys has been examined in a number of density functional calculations. These studies used the local density approximation (LDA), which is known to significantly underestimate the band gaps of semiconductors. Kumar *et al.*[13] attempted to correct for the band gap by using the modified Becke-Johnson functional

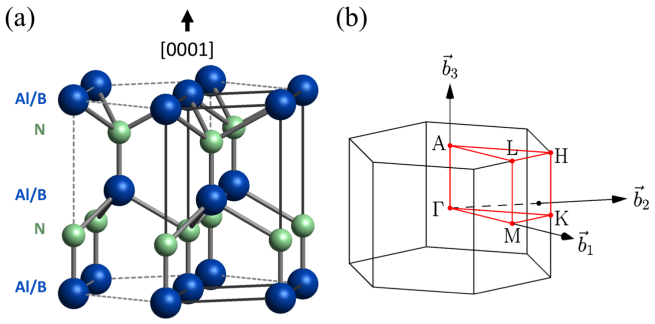

FIG. 1. (Color online) (a) The crystal structure and (b) Brillouin zone of wurtzite AlN and BN. The cation sites (blue) can be occupied by either Al or B, while the anion sites (green) are occupied by N. The solid black lines in (a) indicate the primitive cell and the red lines in (b) indicate the standard high symmetry path.

for their calculations of zinc-blende BAlN alloys. However, the band gaps of the parent compounds were still severely underestimated, affecting a quantitative description of the alloy electronic structure. Zhang *et al.*[14] used a scissor shift to correct the LDA band gaps in their calculations of wurtzite BAlN alloys. However, their procedure for identifying the character of conduction-band extrema is unclear. In addition, some of their alloy band structures included low-dispersion bands that could be indicative of localized states, which can lead to a spurious reduction in the calculated band gap. Our present work overcomes these problems by using a hybrid functional to consistently calculate structural as well as electronic properties of wurtzite $B_xAl_{1-x}N$ alloys. Hybrid density functional theory (DFT) has previously been successfully applied to the parent compounds, wurtzite AlN[15] and hexagonal BN.[4]

Since AlN is a direct-band-gap semiconductor and BN is indirect, a crossover from direct to indirect band gap will occur. If information about the wurtzite phase of BN is available, one can attempt linear interpolation of the band gaps to identify the boron concentration at which the direct-to-indirect crossover occurs. However, we will

see that the direct band gap of BAlN is strongly nonlinear as a function of boron content, i.e., it exhibits a large bowing, while the bowing of the indirect band gap is much weaker. Explicit alloy calculations are therefore essential. We identify the direct and indirect band gaps and predict the direct-to-indirect crossover to occur at 28% boron incorporation. While maintaining a direct gap up to high boron concentration is favorable for optoelectronic applications, a key conclusion from our work is that the value of this gap barely increases above the AlN value.

II. METHODOLOGY

A. First-principles calculations

Our DFT calculations use the hybrid functional of Heyd, Scuseria, and Ernzerhof (HSE)[16] as implemented in the VASP code.[17,18] The mixing parameter α is set to 0.33, which leads to an accurate description of the band gaps and structural properties of the parent compounds, AlN and BN, in their respective ground-state phases. Our calculations use projector augmented wave (PAW) potentials[19] and a plane-wave cutoff energy of 420 eV. For the calculations of the primitive unit cells of the parent compounds we use a $8 \times 8 \times 6$ Γ-centered k-point grid. To account for the Van der Waals interactions in our calculations of hexagonal BN (h-BN) we use the semi-empirical Grimme-D3 method.[20] For the alloy supercell calculations, a $2\times2\times2$ Monkhorst-Pack k-point grid is used.

The calculations of $B_xAl_{1-x}N$ alloys are performed using a $3\times3\times2$ wurtzite supercell that contains 72 atoms. For each boron concentration, we generate ten BAlN alloy structures with a random distribution of B atoms. The lattice mismatch between the two parent compounds is large (19%). The lattice parameters are varied linearly as a function of boron content in accordance with Vegard's law. For example, the in-plane lattice parameter, $a_{B_xAl_{(1-x)}N}$ of the BAlN alloy is:

$$a_{B_xAl_{1-x}N} = x a_{BN} + (1-x) a_{AlN} \quad (1)$$

where x is the boron content, a_{BN} is the in-plane lattice parameter of wurtzite BN (wz-BN) and a_{AlN} is the in-plane lattice parameter of wz-AlN. The atomic positions within the supercell were allowed to relax using HSE until all of the forces are below 20 meV/Å. We verified the accuracy of Vegard's law for a subset of alloy structures by allowing both the lattice parameters and atomic positions to relax. In all cases, the variation in the lattice parameters was close to linear, i.e., it followed Vegard's law.

B. Determination of alloy band edges

The conduction-band minima (CBM) of wurtzite AlN and BN lie at different high-symmetry points in the Brillouin zone (BZ) [Fig. 1(b)]; the CBM is at Γ in AlN and at K in BN. At a critical boron concentration, a direct-to-indirect crossover will occur. The alloy calculations are performed in supercells, which have a smaller Brillouin zone than the parent compounds. Zone folding will occur, which complicates the identification of direct and indirect band gaps in the alloy band structures. Calculations of direct-to-indirect crossovers in alloy band gaps can be based on identifying band degeneracies.[13,21] However, examining the degeneracies is challenging for alloys of wz-AlN because some conduction-band extrema at other high-symmetry points are similar in energy to the value at K, and many supercell configurations will fold these points together. In addition, the large size mismatch between Al and B leads to large lattice relaxations that lower the symmetry and split degeneracies, making it even more challenging to identify conduction band states that correspond to AlN or BN via band degeneracies. To overcome these challenges, we utilize a different approach, which is in the spirit of unfolding the band structure of an alloy supercell by projecting the wave functions onto the supercell of a pure material.[22,23]

Our projection scheme is based on $3\times3\times2$ BAlN alloy supercells and pristine AlN and BN supercells strained to the same size. Since we are interested in BAlN alloys at low B content, we project onto wave functions in an AlN supercell . The K point, which occurs at the corner of the Brillouin zone (1/3,1/3,0) for the 4-atom primitive cell of AlN, is folded to Γ in the $3 \times 3 \times 2$ supercell, as illustrated in Fig. 2.

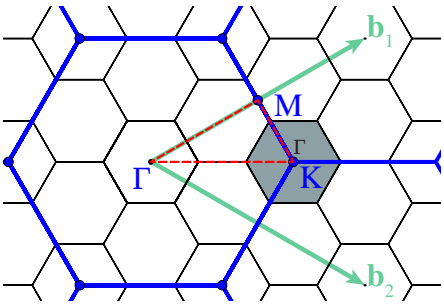

FIG. 2. (Color online) In-plane reciprocal lattice for the wurtzite structure. The Brillouin zone corresponding to the primitive unit cell is indicated in blue, and the reciprocal lattice vectors $\mathbf{b_1}$ and $\mathbf{b_2}$ are shown. The high-symmetry path is shown in red. The Brillouin zone of the $3\times3\times2$ supercell is shown in black. Note that the K point corresponding to the primitive unit cell is folded onto the Γ point of the supercell.

The band structure of the primitive cell of AlN is shown in Fig. 3(a). The conduction-band states at Γ and K (Γ_c and K_c) as well as the valence-band state at Γ (Γ_v) are all folded to Γ (Γ^{AlN}) in the AlN supercell. The supercell states that correspond to states of interest in

the primitive cell can be identified by their eigenenergies, atomic orbital contributions, and degeneracies. For the BAlN supercells, we project the states at Γ ($\Gamma^{\rm SC}$) onto the states of the AlN supercell that we identify with $\Gamma_{\rm v}$, $\Gamma_{\rm c}$ and $\rm K_c$. Each band in the alloy supercell gives us a projection weight defined as:

$$\left|\left\langle \Gamma^{\rm AlN}, n\right|\left. \Gamma^{\rm SC}, m\right\rangle\right| , \quad (2)$$

where $\left|\Gamma^{\rm SC}, m\right\rangle$ is a state at Γ in the BAlN alloy supercell with band index m, and $\left|\Gamma^{\rm AlN}, n\right\rangle$ is one of the states at Γ identified above for the (strained) pristine AlN supercell.

We compute these projection weights for each band index m in the BAlN alloy supercell. This allows us to identify the states at $\Gamma^{\rm SC}$ in the BAlN supercell that have the largest projection weight associated with the $\Gamma_{\rm v}$, $\Gamma_{\rm c}$ and $\rm K_c$ states. Once the states of interest have been identified, the direct band gap is taken to be the energy difference between the eigenvalues of the states that have strongest projection weight onto $\Gamma_{\rm c}$ and $\Gamma_{\rm v}$, and the indirect band gap is given by the energy difference between the eigenvalues of the BAlN states that have the strongest projection weight onto $\rm K_c$ and $\Gamma_{\rm v}$.

To take different atomic arrangements in the alloy into account, ten randomly constructed atomic configurations are generated at each boron content. We do not use Special Quasi-random Structures (SQS)[24] here. While the SQS approach is often productively used to model alloy properties, the shape of the SQS supercell would preclude performing the projections onto states of the parent compounds that allow identifying the states corresponding to the CBM at Γ and K. Full atomic relaxation is allowed for each of our ten random configurations. *Average* direct and indirect band gaps at a given boron content are then obtained by averaging the band gaps calculated for these ten atomic configurations of our alloy supercells. We feel that this approach to determining the band edges approximates the results that would be obtained from experimental measurements that probe the electronic structure of the alloy.

By identifying the direct and indirect band gaps of BAlN as a function of boron content we can evaluate the bowing parameters for each transition. For example, the bowing parameter $b^{\rm dir}$ for the direct band gap of BAlN is defined as:

$$E_g^{\rm dir}({\rm B}_x{\rm Al}_{1-x}{\rm N}) = xE_g^{\rm dir}({\rm BN}) + (1-x)E_g^{\rm dir}({\rm AlN}) - b^{\rm dir}x(1-x) \quad (3)$$

where $E_g^{\rm dir}$(BN) is the direct band gap of wz-BN and $E_g^{\rm dir}$(AlN) is the direct band gap of AlN (both at Γ). A similar bowing parameter can be defined for the indirect band gap using the constituent indirect band gaps (corresponding to the CBM at K) of wurtzite AlN and BN.

III. RESULTS AND DISCUSSION

A. Parent compounds

We first examine the structural and electronic properties of AlN and BN. AlN is stable in the wurtzite structure (Fig. 1). The ground state of BN is the hexagonal structure, in which B and N atoms are arranged in an in-plane, sp^2 bonded honeycomb lattice. The BN layers are weakly bonded to each other by Van der Waals forces in an AB stacking configuration. BN can also be stabilized in the wurtzite structure, which is of primary interest for the present study.

The structural and electronic properties of AlN and BN in the wurtzite and hexagonal phases are summarized in Table I. Our choice of $\alpha = 0.33$ for the HSE mixing parameter yields lattice parameters for wz-AlN and h-BN that are generally within 1% of the experimental parameters for each material, with only a slightly larger deviation (1.5%) for the c lattice parameter of h-BN. We also obtain a direct band gap of 6.18 eV for wz-AlN, which is within the range of experimentally measured gaps (6.12 eV − 6.19 eV).[25,26] For wz-BN, no experimental values are available, but $\alpha = 0.33$ produces an indirect band gap of 5.98 eV for h-BN, very close to the indirect band gap of 6.08 eV[27] measured in bulk h-BN.

The HSE-calculated band structures of wurtzite AlN and BN are shown in Fig. 3. The orbital contribution to the states in the band structure is illustrated by a distinct color: yellow for s-states and purple for p-states. The fundamental band gap of AlN is direct at Γ. The CBM of AlN at Γ is primarily composed of s states while the VBM at Γ is primarily composed of p states. The wurtzite crystal field splits the VBM of AlN into a doubly degenerate Γ_6 and a singly degenerate Γ_1 state. The topmost Γ_1 valence-band state in AlN (labeled Γ_v) has strong p_z character, as evidenced by the isosurface shown in the inset of Fig. 3(a).

Wurtzite BN, unlike AlN, is an indirect band gap semiconductor with the VBM at Γ and CBM at K. For the purposes of expressing the direct and indirect band gaps of BAlN alloys with respect to those of the parent compounds (and extracting bowing parameters) we need to focus on the band gaps of wz-AlN and wz-BN determined relative to the band edges that have the same character. Since we are interested in BAlN alloys with low B content, we focus on identifying valence- and conduction-band states in BN that have the same character as in AlN. In wz-BN, the Γ_1 valence-band state with p_z character occurs at 0.27 eV below the VBM; this state is labeled Γ_v in Fig. 3(b). For the conduction band, the singly degenerate Γ_c conduction-band state in wz-AlN has its equivalent in a state in wz-BN [also labeled Γ_c in Fig. 3(b)] that is composed primarily of s states at 13.90 eV above Γ_v.

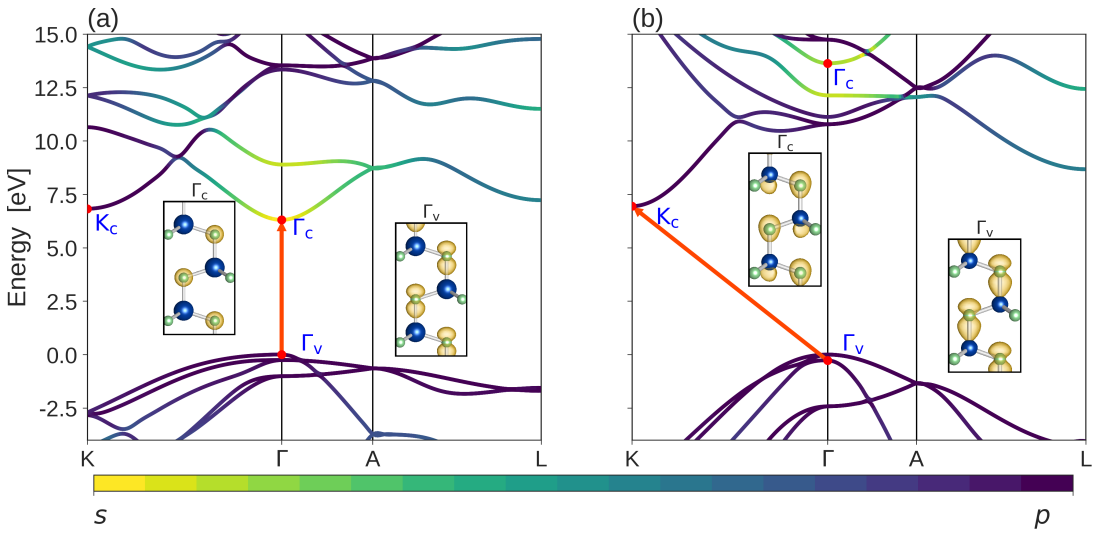

FIG. 3. (Color online) Band structures of wurtzite bulk (a) AlN and (b) BN calculated with the HSE functional. The color of each band indicates the angular momentum character of the states, according to the color bar below the plot. The valence-band maximum (VBM) at Γ was used as the zero-energy reference in each plot. The isosurfaces correspond to the Γ_v and Γ_c wave functions are shown for each material.

TABLE I. Lattice parameters a and c and band gaps E_g of bulk AlN and BN in their wurtzite (wz) and hexagonal (h) phases. Values calculated with the HSE functional are compared with results from experimental studies. The nature of the transition (VBM → CBM) corresponding to the direct and indirect gaps E_g is shown in parentheses. The calculated values for the transitions of interest for the wurtzite materials are shown in the last two columns.

Material	Method	a [Å]	c [Å]	E_g [eV]	$\Gamma_v \rightarrow \Gamma_c$ [eV]	$\Gamma_v \rightarrow K_c$ [eV]
wz-AlN	HSE	3.08	4.93	6.18 (Γ → Γ)	6.18	6.82
	Exp.	3.11[a]	4.98[a]	6.12–6.19[b]	-	-
h-AlN	HSE	3.26	4.10	5.42 (Γ → Γ)	-	-
	Exp.	-	-	-	-	-
wz-BN	HSE	2.52	4.17	6.84 (Γ → K)	13.90	7.21
	Exp.	2.55[c]	4.21–4.22[c]	-	-	-
h-BN	HSE	2.49	6.56	5.98 (∼ H →∼ M)	-	-
	Exp.	2.50–2.51[d]	6.66-6.68[d]	5.75–6.08[e]	-	-

[a] Ref.28
[b] Ref. 25 and 26
[c] Ref. 29 and 30
[d] Ref. 31 and 32
[e] Ref. 27 and 33

B. Alloy structure

In a BAlN alloy, each B and Al cation is tetrahedrally coordinated by four N atoms. In our wz-AlN calculations the Al-N bond length is 1.90 Å for the axial bond along the c-axis and 1.89 Å for the other bonds (which we refer to as planar bonds). In wz-BN the axial bond length is 1.58 Å and the planar bond length 1.56 Å. We have analyzed the distribution of nearest-neighbor Al-N and B-N bond lengths as a function of boron concentration. For each concentration and configuration we average over the planar and axial Al-N and B-N bond lengths. The results are illustrated in Fig. 4 for the lowest and highest boron concentrations investigated in our study. While Fig. 4 shows the bond length averaged over ten atomic configurations, the bond-length distribution for each individual configuration closely resembles the average. The nearest-neighbor bond lengths exhibit a bimodal distribution, peaked near the bond lengths of the parent compounds. For the lowest boron concentration that we investigate ($x = 0.03$) the distribution in the B-N bond lengths is consistent with the bond lengths one would expect from ternary alloys in the dilute limit.[34] As the boron content increases up $x = 0.17$, the distributions of the Al-N and B-N bond lengths are both broadened, as illustrated in Fig. 4.

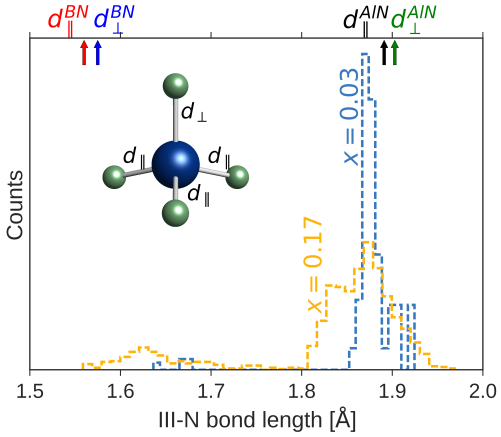

FIG. 4. (Color online) Distribution of nearest neighbor cation-nitrogen bonds for boron concentrations of x=0.03 and x=0.17. The in-plane ($d_{\parallel}$) and out-of-plane ($d_{\perp}$) bond lengths for AlN and BN are indicated on the top axis.

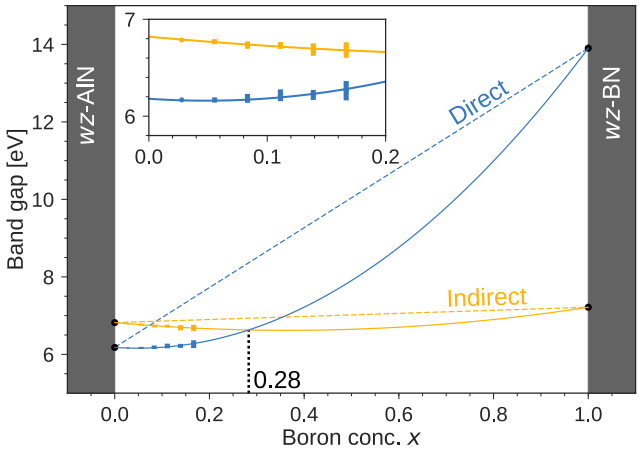

FIG. 5. (Color online) Direct $\Gamma_v \rightarrow \Gamma_c$ and indirect $\Gamma_v \rightarrow K_c$ band gaps of wurtzite $B_xAl_{1-x}N$ alloys as a function of boron concentration x. Linear interpolations of the direct and indirect band gaps are indicated by dashed lines. The spread of calculated values at each concentration is illustrated by the vertical bars. The solid curves indicate a quadratic fit to the calculated data [Eq. (3)]. The crossover between direct and indirect band gap at 28% is indicated by the vertical dotted line. The inset zooms in on the concentration range between 0 and 0.2.

C. Alloy band structure

We now use the projection scheme outlined in Sec. II B to identify the direct and indirect band gaps of $B_xAl_{1-x}N$ alloys. We limit our calculations to a boron content of x=0.17; for higher boron concentrations the band-edge states for the alloy exhibit larger contributions from BN, and our scheme of identifying states based on projecting on AlN states becomes less reliable. We checked for the presence of localized states within the band gap by plotting the wave functions of states in the vicinity of the band edges. Our alloy band structures calculated consistently within HSE do not show any evidence of localized states.

Since AlN has a direct gap and BN an indirect gap, we expect to see a direct-to-indirect crossover in the band gap of wurtzite BAlN alloys at a critical boron concentration. Linear interpolation between the gaps of the parent compounds would place this critical boron concentration at x=0.08 (see Fig. 5). However, alloy band gaps exhibit bowing, which can be particularly large if the lattice mismatch is large, and these nonlinearities will affect the crossover. One expects different bowing parameters [Eq. (3)] for the direct and indirect band gaps of BAlN. A least-squares fit of the calculated BAlN band gaps to a second order polynomial leads to a bowing parameter of 8.55 eV for the direct band gap and a bowing parameter of 1.49 eV for the indirect gap. Using these bowing parameters to describe the alloy band gaps leads to the direct-to-indirect crossover occurring at 28% boron, illustrated by the vertical line in Fig. 5.

The description of the band gap with Eq. (3) using a single bowing parameter is only an approximation, particularly in the case of large lattice mismatch and strong bowing. A better description might be obtained by using a higher-order polynomial; alternatively, a composition-dependent bowing parameter can be defined by determining a value for b based on Eq. (3) at each composition x. It turns out that, over the range of boron concentrations considered in our study, the bowing parameter is not particularly sensitive to the composition. For the direct gap, the bowing parameter $b^{\rm dir}$ varies from 8.38 eV at x=0.03 to 8.67 eV at x=0.17, small variations compared to the value of $b^{\rm dir}$ = 8.55 eV obtained by a fit over the entire range. Similarly, for the indirect gap, the bowing parameter varies from 1.65 eV at x=0.03 to 1.46 eV at x=0.17 (compared to 1.49 eV obtained from the full-range fit). We conclude the direct and indirect band gaps of the BAlN band gaps are well described by a single bowing parameter.

The spread (standard deviation) in the direct and indirect band gaps for each set of atomic configurations at a given boron content is illustrated in the inset of Fig. 5, and tabulated in Table II. For boron concentrations up to 17% this spread is quite small. At the lowest simulated boron concentration (x =0.03) only one Al atom in the supercell is replaced by B, which means that only a single atomic configuration needs to be calculated. At the next boron concentration (x =0.06), the spread in band-gap values is still very low. The band-gap value in the structure where the boron atoms are furthest apart compared to the structure where the boron atoms are closest together (i.e., on nearest-neighbor cation sites) is 41 meV higher for the direct band gap and 62 meV higher for the indirect band gap. At x=0.17 the spread in the direct band gap is 100 meV and the spread in the indirect band gap is 80 meV.

The success of our projection scheme is based on our

ability to project states of the alloy onto states of AlN and thus distinguish states that have Γ_c and K_c character. As an example, for the K_C state, the (normalized) magnitude of the projection [Eq. (2)] goes from 0.98 at x=0.03 to 0.53 at x =0.17. This is of course accompanied by an increased energy spread of the projections, but this distribution is quite peaked and for concentrations up to x=0.17 this provides an unambiguous identification of the band edges. For concentrations beyond x=0.17 the magnitude of the projections onto the AlN states decreases since the conduction-band states attain more contributions from BN. Hence, our ability to clearly distinguish between Γ_c and K_c states decreases. For this reason, we limit our calculations to a concentration of 17% boron.

TABLE II. Standard deviation of the computed direct and indirect band gaps in units of meV.

x	0.03	0.06	0.08	0.11	0.14	0.17
direct	0	26	46	61	52	100
indirect	0	25	37	35	65	80

D. Implications for applications of BAlN alloys

Finally, we comment on the implications of our results for applications of BAlN alloys. Our calculations indicate it is possible to maintain a direct band gap of the BAlN alloy up to x=0.28, a much larger concentration than would be estimated based on simple linear interpolation.

However, it is doubtful that this actually offers any benefit in the case of optoelectronic devices, where an important goal would be to increase the band gap above the AlN value. We find that, due to large band-gap bowing, the band gap is actually slightly *reduced* at low B concentrations (by 0.02 eV at x=0.05). After that it increases only by a nominal amount before reaching the direct-to-indirect crossover at x=0.28, where an increase of the direct gap by 0.45 eV is calculated. Since BAlN alloys probably exhibit poor miscibility due to the large lattice mismatch between AlN and BN,[10] it is doubtful that at the B concentrations for which homogeneous alloys can be achieved any increase in band gap will be observed.

Finally, we note that the band edges of BAlN alloys may be sensitive to the effects of short-range order.[35] These effects could be explored in future work if experimental evidence for short-range order emerges.

IV. CONCLUSIONS

We have investigated the structural and electronic properties of wurtzite BAlN alloys using first-principles calculations based on hybrid density functional theory and a projection scheme to identify band edges. We find a large bowing of the direct band gap (bowing parameter b^{dir}=8.55 eV) for the direct band gap and a weaker bowing (b^{ind}=1.49 eV) for the indirect band gap. Our results indicate that BAlN alloys will have a direct band gap up to a boron concentration of x=0.28, a much larger concentration than would be estimated based on linear interpolation. However, the increase in the direct gap over the AlN value is very modest.

ACKNOWLEDGMENTS

J. S. was supported by the National Science Foundation (NSF) under Grant No. DMR-143485. D. W. was supported by the U. S. Department of Energy (DOE), Office of Science, Basic Energy Sciences (BES) under Award No. DE-SC0010689. Computational resources were provided by the Extreme Science and Engineering Discovery Environment (XSEDE), supported by the NSF (ACI-1548562).

[1] S. Nakamura and M. R. Krames, Proc. IEEE **101**, 2211 (2013).
[2] A. Pourhashemi, R. M. Farrell, D. A. Cohen, J. S. Speck, S. P. DenBaars, and S. Nakamura, Appl. Phys. Lett. **106**, 111105 (2015).
[3] U. Mishra, P. Parikh, and Yi-Feng Wu, Proc. IEEE **90**, 1022 (2002).
[4] C. E. Dreyer, J. L. Lyons, A. Janotti, and C. G. Van De Walle, Appl. Phys. Express **7** (2014).
[5] C. E. Dreyer, A. Janotti, C. G. Van de Walle, and D. Vanderbilt, Phys. Rev. X **6**, 021038 (2016).
[6] R. Geick, C. H. Perry, and G. Rupprecht, Phys. Rev. **146**, 543 (1966).
[7] X. Li, S. Sundaram, Y. El Gmili, F. Genty, S. Bouchoule, G. Patriache, P. Disseix, F. Réveret, J. Leymarie, J.-P. Salvestrini, R. D. Dupuis, P. L. Voss, and A. Ougazzaden, J. Cryst. Growth **414**, 119 (2015).
[8] A. Nakajima, Y. Furukawa, H. Yokoya, and H. Yonezu, J. Cryst. Growth **278**, 437 (2005).
[9] T. L. Williamson, N. R. Weisse-Bernstein, and M. A. Hoffbauer, Phys. Status Solidi **11**, 462 (2014).
[10] L. K. Teles, L. M. R. Scolfaro, J. R. Leite, J. Furthmüller, and F. Bechstedt, Appl. Phys. Lett. **80**, 1177 (2002).
[11] J.-C. Zheng, H.-Q. Wang, C. H. A. Huan, and A. T. S. Wee, J. Phys. Condens. Matter **13**, 5295 (2001).
[12] L. Teles, J. Furthmüller, L. Scolfaro, A. Tabata, J. Leite, F. Bechstedt, T. Frey, D. As, and K. Lischka, Phys. E Low-dimensional Syst. Nanostructures **13**, 1086 (2002).
[13] S. Kumar, S. Joshi, B. Joshi, and S. Auluck, J. Phys. Chem. Solids **86**, 101 (2015).

[14] M. Zhang and X. Li, Phys. Status Solidi **254**, 1600749 (2017).
[15] J. L. Lyons, A. Janotti, and C. G. Van de Walle, Phys. Rev. B **89**, 035204 (2014).
[16] J. Heyd, G. E. Scuseria, and M. Ernzerhof, J. Chem. Phys. **124**, 219906 (2006).
[17] G. Kresse and J. Furthmüller, Phys. Rev. B **54**, 11169 (1996).
[18] G. Kresse and J. Furthmüller, Comput. Mater. Sci. **6**, 15 (1996).
[19] P. E. Blöchl, Phys. Rev. B **50**, 17953 (1994).
[20] S. Grimme, J. Antony, S. Ehrlich, and H. Krieg, J. Chem. Phys. **132**, 154104 (2010).
[21] J. W. Nicklas and J. W. Wilkins, Appl. Phys. Lett. **97**, 091902 (2010).
[22] V. Popescu and A. Zunger, Phys. Rev. B **85**, 085201 (2012).
[23] Y. Zhang, A. Mascarenhas, and L.-W. Wang, Phys. Rev. B **78**, 235202 (2008).
[24] S.-H. Wei, L. G. Ferreira, J. E. Bernard, and A. Zunger, Phys. Rev. B **42**, 9622 (1990).
[25] J. Li, K. B. Nam, M. L. Nakarmi, J. Y. Lin, H. X. Jiang, P. Carrier, and S.-H. Wei, Appl. Phys. Lett. **83**, 5163 (2003).
[26] D. Brunner, H. Angerer, E. Bustarret, F. Freudenberg, R. Hopler, R. Dimitrov, O. Ambacher, and M. Stutzmann, J. Appl. Phys. **82**, 5090 (1997).
[27] G. Cassabois, P. Valvin, and B. Gil, Nat. Photonics **10**, 262 (2016), 1512.02962.
[28] S. Iwama, K. Hayakawa, and T. Arizumi, J. Cryst. Growth **56**, 265 (1982).
[29] A. Nagakubo, H. Ogi, H. Sumiya, K. Kusakabe, and M. Hirao, Appl. Phys. Lett. **102**, 241909 (2013).
[30] V. L. Solozhenko, D. Hausermann, M. Mezouar, and M. Kunz, Appl. Phys. Lett. **72**, 1691 (1998).
[31] Y. Andreev and T. Lundström, J. Alloys Compd. **216**, L5 (1994).
[32] V. L. Solozhenko, High Press. Res. **13**, 199 (1995).
[33] D. A. Evans, A. G. McGlynn, B. M. Towlson, M. Gunn, D. Jones, T. E. Jenkins, R. Winter, and N. R. J. Poolton, J. Phys. Condens. Matter **20**, 75233 (2008).
[34] C. K. Shih, W. E. Spicer, W. A. Harrison, and A. Sher, Phys. Rev. B **31**, 1139 (1985).
[35] L. Bellaiche and A. Zunger, Phys. Rev. B **57**, 4425 (1998).